Processing and Application of Ceramics 11 [4] (2017) 258–264
https://doi.org/10.2298/PAC1704258M

Preparation, dielectric and conductivity studies of $LiNi_{1-x}Mg_xO_2$ cathode materials for lithium-ion batteries

Nandigam Murali[1,2,*], Valaparla Veeraiah[2]

[1]*Advanced Analytical Laboratory, DST-PURSE Programme, Andhra University, Visakhapatnam-530 003, India*
[2]*Department of Physics, Andhra University, Visakhapatnam-530 003, India*

Received 30 July 2016; Received in revised form 12 November 2016; Received in revised form 25 April 2017; Received in revised form 29 August 2017; Accepted 26 September 2017

Abstract

A layered structure cathode materials $LiNi_{1-x}Mg_xO_2$ (where x = 0.0 and 0.02) were prepared by solid state reaction from Li_2CO_3, MgO and NiO. The thermal analysis of the precursor materials up to 750 °C showed the weight loss of about 30%. The X-ray diffraction patterns of the synthesized samples confirmed the presence of α-$NaFeO_2$ structure with the rhombohedral-hexagonal symmetry (space group, $R\bar{3}m$) and no evidence of any impurities. The peaks intensity ratio I_{003}/I_{104} increased with Mg concentration, which indicates the cation mixing within transition metal layer and lithium layer. The Fourier transform infrared spectroscopy showed the presence of two broad vibrational bands between 400 and 1000 cm^{-1} and corresponding bands for the 3a and 3b octahedral sites of LiO_6 and MO_6 units. The scanning electron microscopy analyses showed that the prepared samples have porous and relatively uniform distribution of grain sizes in the range 0.4–3μm. The complex impedance spectroscopy studies of the samples sintered at 850 °C were done in the frequency range from 42 Hz to 1 MHz with temperature variation from 30 to 100 °C. The results revealed that the total electrical conductivity increases with temperature and frequency and at 100 °C it is 7.06×10^{-6} and 9.00×10^{-6} S/cm for the $LiNiO_2$ and $LiNi_{1-x}Mg_xO_2$ materials, respectively. The obtained relatively high conductivity and low dielectric constant confirmed that the prepared ceramics can be used as cathode materials for Li-ion batteries.

Keywords: *$LiNiO_2$, layered structure, XRD, FESEM, FT-IR, dielectric constant, conductivity*

I. Introduction

Ceramic cathode materials are currently used in most of the commercially available lithium-ion batteries. They have wide applications, such as in electronic mobile devices and electric vehicles [1–6]. The cathode materials are primarily categorized based on their structure, those having layered structures ($LiCoO_2$, $LiNiO_2$ and $LiMnO_2$), olivine structure ($LiFePO_4$ based materials) and spinel structure ($LiMn_2O_4$ with three-dimensional framework structure) [7–11]. In the past decades, the layered structure $LiCoO_2$ cathode material was commercially used very successfully. However, $LiCoO_2$ has a high manufacturing cost and insufficient reversible capacity of 140 mA h/g [12]. One of the most promising alternative materials for resolving these issues is $LiNiO_2$ [13]. Recently, $LiNiO_2$ has been the most widely used cathode material in commercial Li-ion batteries because of its high discharge capacity, low cost and environmentally acceptable properties. However, it is difficult to obtain stoichiometric $LiNiO_2$ by solid-state reaction method at high temperature in air atmosphere. The difficulty in synthesizing stoichiometric $LiNiO_2$ is also due to the loss of lithium from the host structure during high temperature calcinations because of the high vapour pressure of lithium, thus leading to the formation of non-stoichiometric structure [14]. This results in a lower initial capacity as well as severe capacity loss upon cycling. Another problem is that its capacity fades, observed even for the stoichiometrically pure $LiNiO_2$, due to the formation of inactive NiO_2 phase. NiO_2 phase is formed due to the irreversible phase transitions occurring in $LiNiO_2$ structure when charging up to a high voltage. Hence, for these reasons, $LiNiO_2$ is

*Corresponding author: tel: +91 9703 725707,
fax: +91 0891 2755324, e-mail: *muraliphdau@gmail.com*

represented as Li_xNiO_2 where x in this case indicates the non-stoichiometry [15,16]. The problem might be solved with substitutions. Thus, in $LiNi_{0.5}Co_{0.5}O_2$ material, cobalt substitution can decrease cation mixing and stabilize the layered structure [17].

In the present work, $LiNi_{1-x}Mg_xO_2$ (where x = 0.0 and 0.02) cathode materials were fabricated at 850 °C for 20 h. An investigation of the structural, morphological and electrical properties of the synthesized materials was performed.

II. Experimental procedure

The cathode materials were synthesized by a solid-state reaction method from stoichiometric amounts of Li_2CO_3 (Merck, 99.9%), MgO (Merck, 99.9%) and NiO (Merck, 99.9%). A slight excess amount of lithium (5%) was used to compensate for any loss of the metal that might have occurred during the calcination at high temperatures. The starting materials were sufficiently mixed, ground and heat treated in air at 500 °C for 5 h. In the second step, the obtained powder was again ground, mixed and calcined at 750 °C for 20 h. Then, the prepared particles were cooled at the rate of 5 °C/min. Finally, the powder was ground, mixed and calcined at 850 °C for 20 h in air using a muffle box furnace. The pellets (with diameter of 10 mm and thickness of 1.1 to 1.25 mm) were also prepared first by mixing the sample and PVA in an agate mortar and pestle for one hour and then by pressing with hydraulic press at 5 t for 6 minutes. The pressed pellets were then sintered at 850 °C for 20 hours.

TG/DTA measurements were conducted using Mettler Toledo TG/DTA 851e instrument from room temperature to 1000 °C in nitrogen atmosphere at the heating rate of 10 °C/min. The phase identification and crystal structure characteristics were determined by X-ray diffraction (XRD) using a Rigaku Cu-Kα diffractometer with diffraction angles between 20 and 80° at the wavelength of 1.5406 Å. The morphologies of the synthesized materials were studied by scanning electron microscopy (FE-SEM, Carl Zeiss, EVO MA 15, Oxford Instruments). The Fourier transform infrared spectra were recorded using Nicolet 6700 using KBr pressed pellet technique. The impedance study on the sintered pellets was performed by a Hioki 3532-50 LCR Hitester in the frequency range 42 Hz to 1 MHz at temperature range from room temperature to 100 °C. The surface layers of the sintered pellets were carefully polished, washed with acetone and coated with silver paste to obtain electrodes.

III. Results and discussion

3.1. Thermal analysis

TG/DTA analyses of the precursor mixtures ($LiNi_{1-x}Mg_xO_2$ where x = 0.0 and 0.02) are presented in Fig. 1. As it can be seen, there is a little change in the weight loss as the result of Mg substitution. The weight loss from room temperature to 150 °C can be related to the loss of water absorbed on the surfaces and some intercalated water molecules that are bonded to hydroxyl groups. The endothermic peaks around 200–250 °C in nitrogen atmosphere were due to the decomposition of $M(OH)_2$ (M = Ni and Mg) to spinel phase M_3O_4 [18,19]. The exothermic peaks around 300–400 °C resulted from the decomposition reaction of Li_2CO_3 to Li_2O. The hexagonal phased $LiNiO_2$ and doped cathode material are formed at higher temperatures. The weight loss was almost zero after 750 °C, which indicated that the phase formation of $LiNi_{1-x}Mg_xO_2$ (where x = 0.0 and 0.02) was completed at this temperature [20].

3.2. XRD analysis

X-ray diffraction patterns of the $LiNiO_2$ and $LiNi_{0.98}Mg_{0.02}O_2$ pellets heat treated at 850 °C are

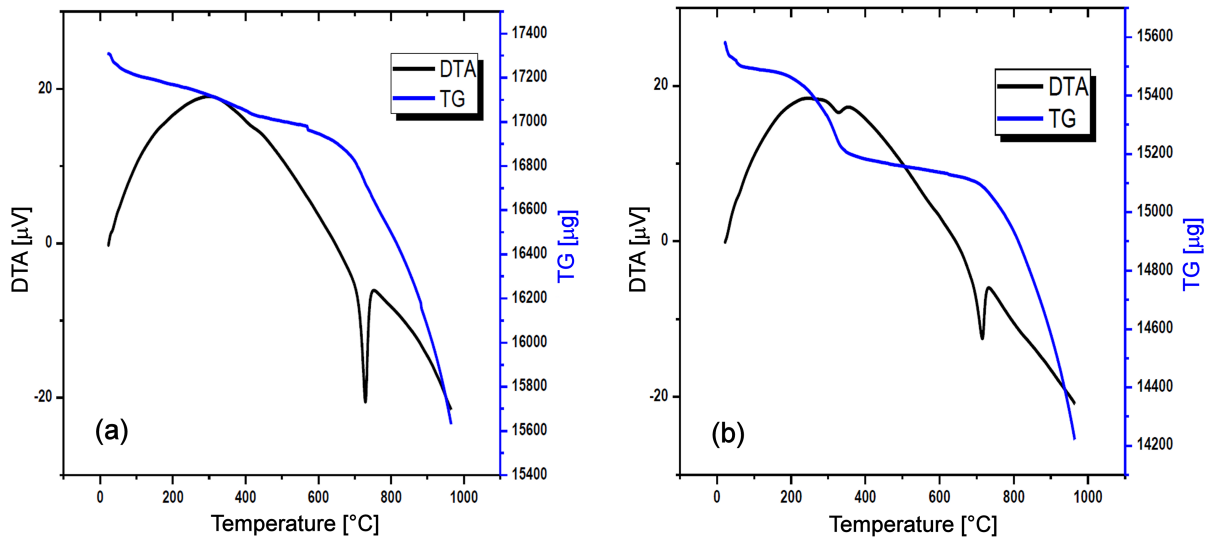

Figure 1. TG/DTA curves of precursor mixture: a) $LiNiO_2$ and b) $LiNi_{0.98}Mg_{0.02}O_2$

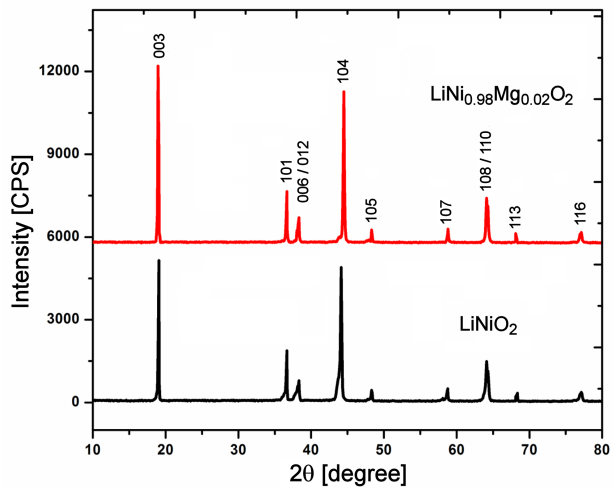

Figure 2. XRD patterns of $LiNiO_2$ and $LiNi_{0.98}Mg_{0.02}O_2$ sintered at 850 °C/20 h

shown in Fig. 2. The XRD spectra showed that both samples have a typical $LiNiO_2$ layered structure without any impurity peaks. The intensity *vs.* diffraction angle peak data showed the similarity to a hexagonal (α-$NaFeO_2$) structure [21,22]. All peaks appearing in the XRD patterns were identified with the characteristic $LiNiO_2$ peaks of the Joint Committee on Powder Diffraction Standards (JCPDS) as well as previously reported works [23,24]. The lattice constants of the synthesized materials were calculated by the Unit-Cell software [25] and listed in Table 1. The Mg substitution resulted in slight changes of the lattice constants, i.e. a increases from 2.865 to 2.870 and c increases from 14.24 to 14.28. The most intensive XRD peaks corresponding to the planes (003), (101) and (104) suggested the well-defined layered structure.

Generally, the oxygen sub-lattice in the α-$NaFeO_2$ hexagonal structure forms a closely packed face centred cubic (*fcc*) lattice with a distortion in the c-direction, which confirms the compound to be hexagonal [26]. The presence of distortion in the c-direction of the $LiNiO_2$ compound was confirmed by the peak splitting at 2θ ~37° and ~64°. This corresponds to (006) (012) and (108) (110) plane doublets, respectively. For the prepared materials, the strongest XRD line was observed for (003) plane. The integrated intensity ratio I_{003}/I_{104} and the split of XRD lines 012 and 110 might serve as a reliable quantitative criterion for the determination of electrochemical activity of $LiNiO_2$. Both materials, $LiNiO_2$ and $LiNi_{0.98}Mg_{0.02}O_2$, showed a high I_{003}/I_{104} value and a clear splitting of XRD lines [27]. The intensity ratio (I_{003}/I_{104}) is an indicator of the degree of displacement of ions between lithium layers (at 3a site) and transition metal layers (at 3b site). If this ratio was in the range of 1.2 to 1.6, it indicated cation mixing/disorder which lead to poor electrochemical performance of the battery [28]. In the present work, the observed intensity ratios (I_{003}/I_{104}) for the prepared $LiNiO_2$ and $LiNi_{0.98}Mg_{0.02}O_2$ compounds are 1.05 and 1.17, which indicate reasonably good electrochemical performance. The value of $(I_{006} + I_{012})/I_{101}$ is called R-factor, which is known to be smaller when the hexagonal ordering is high. This value was useful to measure the cation disorder. As it can be seen from Table 1, the R-factor for $LiNiO_2$ and $LiNi_{0.98}Mg_{0.02}O_2$ are 0.5 and 0.46, respectively, suggesting that the hexagonal ordering is good [29].

3.3. SEM analysis

The grain size and surface morphology of the materials sintered at 850 °C were investigated by scanning

Table 1. Lattice parameter (a and c), unit cell volume (V), R-factor, I_{003}/I_{104} and crystallite size (D) of $LiNiO_2$ and $LiNi_{0.98}Mg_{0.02}O_2$

Compound	a [Å]	c [Å]	V [Å^3]	c/a	R-factor	I_{003}/I_{104}	D [nm]
$LiNiO_2$	2.865	14.24	101.67	4.97	0.50	1.05	10.8
$LiNi_{0.98}Mg_{0.02}O_2$	2.870	14.28	101.78	4.98	0.46	1.17	8.5

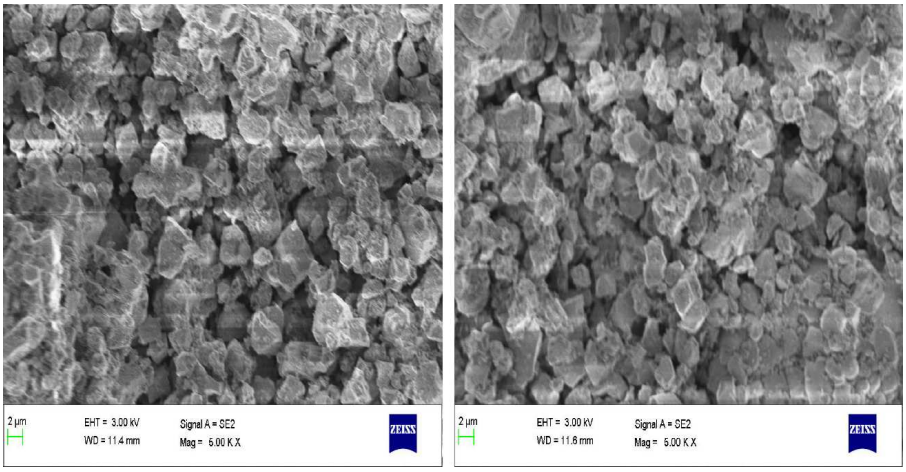

Figure 3. FE-SEM images of: a) $LiNiO_2$ and b) $LiNi_{0.98}Mg_{0.02}O_2$ sintered at 850 °C/20 h

Table 2. FTIR wavenumber variation between $LiNiO_2$ and $LiNi_{0.98}Mg_{0.02}O_2$

Compound	Wavenumbers [cm^{-1}]						
$LiNiO_2$	419.318	440.567	458.983	473.149	481.649	532.14	608.13
$LiNi_{0.98}Mg_{0.02}O_2$	419.318	441.256	458.983	473.2456	481.756	532.14	608.13

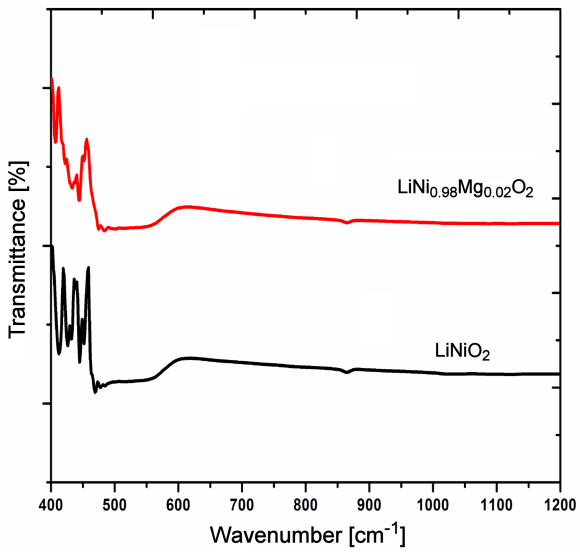

Figure 4. FTIR spectra of $LiNiO_2$ and $LiNi_{0.98}Mg_{0.02}O_2$

electron microscopy (FE-SEM). Figure 3 showed that the prepared samples have porous microstructure and relatively uniform distribution of grain sizes. The sintered $LiNi_{0.98}Mg_{0.02}O_2$ sample has a somewhat coarser structure, which could be caused by Mg addition. The average grain sizes were estimated to be between 2.7 μm and 3.2 μm for $LiNiO_2$ and $LiNi_{0.98}Mg_{0.02}O_2$. This unique morphology is advantageous for electrode materials, because it allows improved electrochemical performances [30,31].

3.4. FTIR studies

Typical FTIR spectra of the $LiNi_{1-x}Mg_xO_2$ (x = 0.0 and 0.02) cathode materials are depicted in Fig. 4. The FTIR spectra display the predominance of the stretching modes and the IR resonance frequency of LiO_6 octahedra located between 400 and 460 cm^{-1}. There are four infrared active vibrations $2A_{2u} + 2E_u$ for the D^5_{3d} group based on group theory analysis [32]. The Wyckoff sites 3a and 3b consist of Li and transition metal cations (i.e. Ni and Mg), respectively. Thus, the separation into LiO_2 and MO_2 mode layers could be seen. The band observed around 532 cm^{-1} was assigned to the asymmetric stretching modes of M–O bonds in MO_6 octahedra and the other band around 608.13 cm^{-1} was attributed to the O–M–O bending modes [33,34]. The broadening of FTIR bands is due to the cation mixing in the crystal layers. When Mg substitution increased, the stretching and bending mode frequencies slightly shifted to higher wavenumber regions, which attributed to changes in covalent character of M–O bond.

3.5. Impedance spectroscopy studies

The electrochemical impedance spectroscopy (EIS) technique was used to study the electrode materials because it can reveal the relationship between the crystal lattice and the electrochemical properties [35]. In complex impedance plot the semi-circle at lower frequencies is due to the contribution of electrode-material interface. Another semicircular arc at intermediate frequencies is due to the contribution of grain boundary and at high frequencies the semicircular arc is due to the bulk response of the material [36,37].

Figure 5 shows Nyquist plots of the $LiNiO_2$ and $LiNi_{0.98}Mg_{0.02}O_2$ electrodes during the course of Li deintercalation. The presence of semicircular arcs is clearly visible. The high Z' and Z'' values at lower frequency regions are due to the higher polarization caused

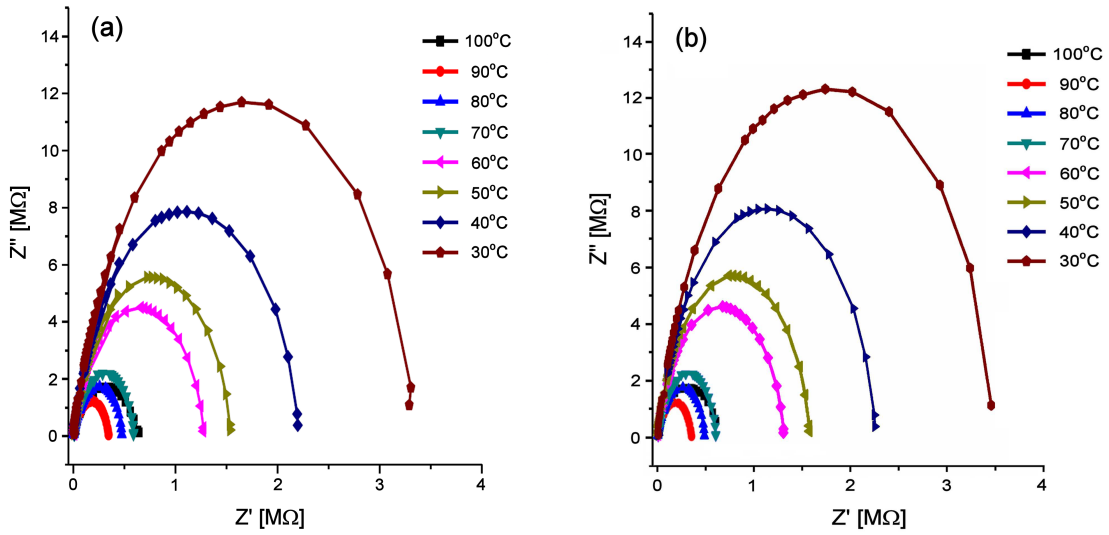

Figure 5. Nyquist plots of: a) $LiNiO_2$ and b) $LiNi_{0.98}Mg_{0.02}O_2$

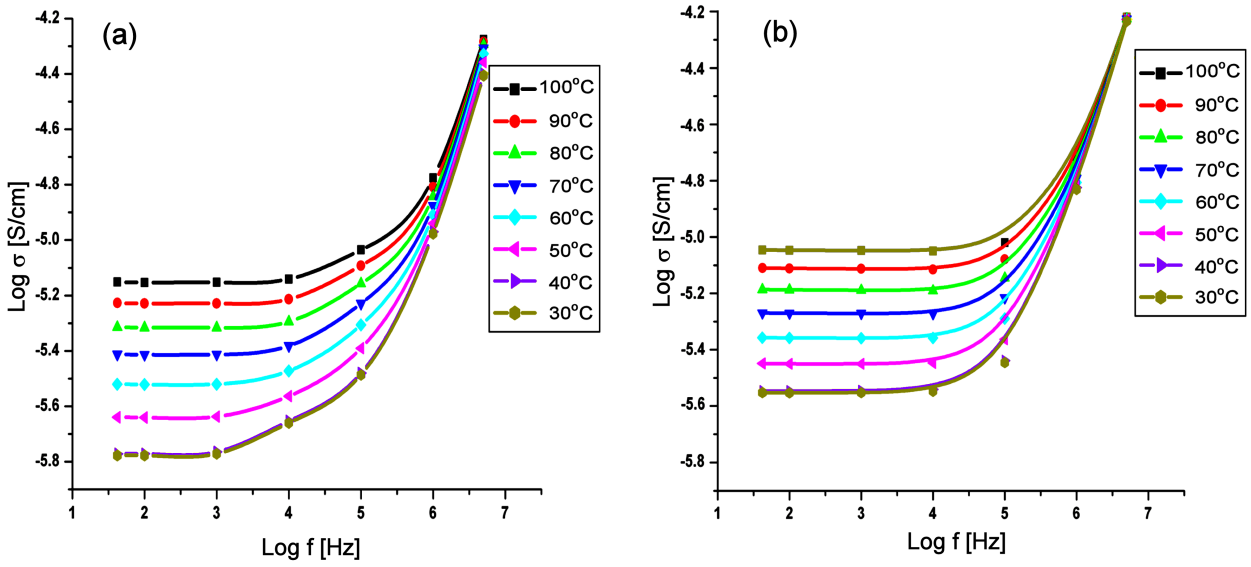

Figure 6. Variation of log σ with frequency plots of: a) $LiNiO_2$ and b) $LiNi_{0.98}Mg_{0.02}O_2$

by space charge. It was also observed that the values of Z' and Z'' gradually decrease with the increase of frequency and temperature, which indicated an increase in AC conductivity with increasing temperature and frequency. In addition, the observed decrease of Z' values at low frequency decreased with the increase in temperature showing negative temperature coefficient of resistance (NTCR) type of behaviour similar to semiconductors [38].

The conductivity of the electrode is considered as a characteristic measure for the cathode performance. However, the electronic properties of cathode materials have not been widely reported. In the previous studies on cathode materials it was established that manufacturing methods affect the conductivity properties [39]. In this study the real and imaginary parts of impedance were evaluated as a function of frequency. The data collected were analysed in the form of impedance plots. From the impedance plots, we obtained bulk resistance of the sample. Finally, AC conductivity was calculated by using the relation:

$$\sigma = \frac{t}{R \cdot a} \tag{1}$$

where t is the thickness, a is the area of cross-section and R is the bulk resistance of the sample.

The frequency dependence of AC conductivity of the $LiNi_{1-x}Mg_xO_2$ (x = 0.0 and 0.02) compounds were presented in Fig. 6 and only the corresponding σ_{AC} values for different temperatures at frequency of 42 Hz were listed in Table 3. The conductivity of the cathode increased with an increase in the temperature. The highest electrical conductivity for $LiNiO_2$ and $LiNi_{0.98}Mg_{0.02}O_2$ was found to be 7.06×10^{-6} and 9.00×10^{-6} S/cm, respectively. The results showed increase of the electrical conductivity in the Mg substituted compound. This was attributed to the weak Ni–O bond strength compared to Mg–O bond.

Table 3. AC conductivity values for $LiNiO_2$ and $LiNi_{0.98}Mg_{0.02}O_2$

Temperature	AC conductivity [$\times 10^6$ S/cm]	
[°C]	$LiNiO_2$	$LiNi_{0.98}Mg_{0.02}O_2$
30	1.67	2.80
40	1.70	2.85
50	2.29	3.56
60	3.02	4.39
70	3.87	5.38
80	4.85	6.51
90	5.92	7.77
100	7.06	9.00

3.6. *Dielectric properties*

The dielectric properties as a function of frequency reflected the dynamic response of the constituents of the material. The relative dielectric constant ε_r of both samples was measured by the capacitance method based on the following equation:

$$\varepsilon = \frac{C \cdot L}{\varepsilon_0 \cdot A} \tag{2}$$

where $\varepsilon_0 = 8.854 \times 10^{-14}$ F/cm is the permittivity of free space, C is the measured capacitance, L and A are the sample thickness and electrode area respectively. The frequency dependences of the dielectric constant (ε_r) of the sintered $LiNi_{1-x}Mg_xO_2$ (x = 0.0 and 0.02) are shown in Fig. 7. The recommended cathode materials for Li-ion batteries should have a low dielectric constant and high conductivity. As it can be seen (Fig. 7), the dielectric constant of the sintered cathode materials ($LiNiO_2$ and $LiNi_{0.98}Mg_{0.02}O_2$) are relatively low. The obtained low value of dielectric constant and relatively low resistance can be used as criteria for choosing the cathode materials for use in Li-ion batteries [42].

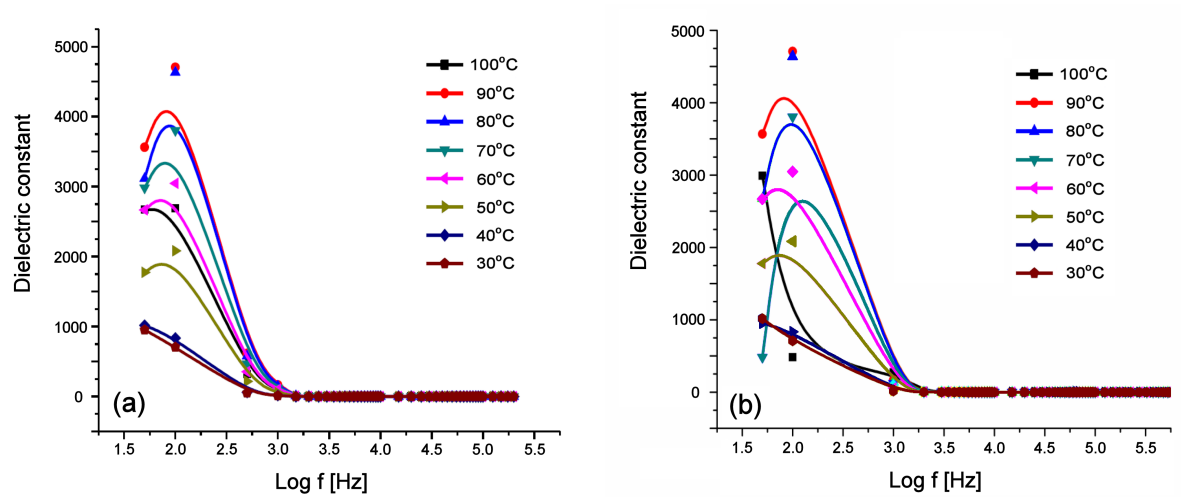

Figure 7. Frequency dependence of the dielectric constant (ε_r) plots of: a) $LiNiO_2$ and b) $LiNi_{0.98}Mg_{0.02}O_2$

IV. Conclusions

$LiNi_{1-x}Mg_xO_2$ (x = 0.0 and 0.02) cathode materials were synthesized by solid state reaction method and sintered at 850 °C for 20 hours. The microstructure, morphology and bonding nature of the synthesized materials were characterized by TG/DTA, XRD, FESEM and FTIR. The intensity *vs*. diffraction angle peak data showed presence of the hexagonal α-$NaFeO_2$ structure (with space group $R\bar{3}m$) without any impurity phase. SEM and FTIR analyses confirm presence of uniform $LiNiO_2$ layered structure with the average grain size if about 3 μm. The AC conductivity of the $LiNiO_2$ and $LiNi_{0.98}Mg_{0.02}O_2$ compounds at 100 °Cwas found to be 7.06×10^{-6} and 9.00×10^{-6} S/cm, respectively. This together with low value of dielectric constant confirms that the prepared ceramics can be used as cathode materials for Li-ion batteries.

References

1. K. Kang, Y.S. Meng, J. Breger, C.P. Grey, G. Ceder, "Electrodes with high power and high capacity for rechargeable lithium batteries", *Science*, **311** (2006) 977–980.
2. A. Manthiram, A. Vadivel Murugan, A. Sarkar, T. Muraliganth, "Nanostructured electrode materials for electrochemical energy storage and conversion", *Energy Environ. Sci.*, **1** (2008) 621–638.
3. S.D. Jones, J.R. Akridge, F.K. Shokoohi, "Thin film rechargeable Li batteries", *Solid State Ionics*, **69** (1994) 357–368.
4. R.M. Dell, "Batteries: Fifty years of materials development", *Solid State Ionics*, **134** (2000) 139–158.
5. Y. Kim, "Lithium nickel cobalt manganese oxide synthesized using alkali chloride flux: Morphology and performance as a cathode material for lithium ion batteries", *ACS Appl. Mater. Interfaces*, **4** (2012) 2329–2333.
6. C. Fu, G. Li, D. Luo, Q. Li, J. Fan, L. Li, "Nickel-rich layered microspheres cathodes: Lithium/nickel disordering and electrochemical performance", *ACS Appl. Mater. Interfaces*, **6** (2014) 15822–15831.
7. R. Ruffo, C. Wessells, R.A. Huggins, Y. Cui, "Electrochemical behavior of $LiCoO_2$ as aqueous lithium-ion battery electrodes", *Electrochem. Commun.*, **11** (2009) 247–249.
8. N. Murali, K. Vijaya Babu, K. Ephraim Babu, V. Veeraiah, "Preparation and structural stability of $LiNiO_2$ in separate synthesis methods at different temperatures", *Chem. Sci. Trans.*, **3** [4] (2014) 1318–1325.
9. C. Liu, J. Nan, X. Zuo, X. Xiao, D. Shu, "Synthesis and electrochemical characteristics of an orthorhombic $LiMnO_2$ cathode material modified with poly(vinylpyrrolidone) for lithium ion batteries", *Int. J. Electrochem. Sci.*, **7** (2012) 7152–7164.
10. T.V.S.L. Satyavani, A. Srinivas Kumar, P.S.V. Subba Rao, "Methods of synthesis and performance improvement of lithium iron phosphate for high rate Li-ion batteries: A review", *Int. J. Eng. Sci. Technol.*, **19** (2016) 178–188.
11. P.T. Shibeshi, V. Veeraiah, "Structural, electrical and electrochemical characterization of $LiLa_{0.01}Cr_{0.13}Mn_{1.86}O_4$ cathode material for lithium-ion battery", *J. Phys. Chem. Solids*, **75** (2014) 1075–1079.
12. W. Liu, P. Oh, X. Liu, M.J. Lee, W. Cho, S. Chae, "Nickel-rich layered lithium transition-metal oxide for high-energy lithium-ion batteries", *Angew. Chem. Int. Ed.*, **54** (2015) 4440–4457.
13. H. Konishi, M. Yoshikawa, T. Hirano, "The effect of thermal stability for high-Ni-content layer-structured cathode materials, $LiNi_{0.8}Mn_{0.1-x}Co_{0.1}Mo_xO_2$ (x = 0, 0.02, 0.04)", *J. Power Sources*, **244** (2013) 23–28.
14. Y. Sun, P. Wan, J. Pan, C. Xu, X. Liu, "Low temperature synthesis of layered $LiNiO_2$ cathode material in air atmosphere by ion exchange reaction", *Solid State Ionics*, **177** (2006) 1173–1177.
15. M. Broussely, F. Perton, P. Biensan, J.M. Bodet, J. Labat, A. Lecerf, C. Delmas, A. Rougier, J.P. Peres, "Li_xNiO_2, a promising cathode for rechargeable lithium batteries", *J. Power Sources*, **54** (1995) 109–114.
16. M.V. Reddy, G.V. Subba Rao, B.V.R. Chowdari, "Preparation and characterization of $LiNi_{0.5}Co_{0.5}O_2$ and $LiNi_{0.5}Co_{0.4}Al_{0.1}O_2$ by molten salt synthesis for Li ion batteries", *J. Phys. Chem. C*, **111** (2007) 11712–11720.
17. G.Y. Kim, Y.J. Park, K.H. Jung, D.J. Yang, J.W. Lee, H.G. Kim, "High rate, high capacity ZrO_2 coated $Li[Li_{1/6}Ni_{1/6}Mn_{1/2}Co_{1/6}]O_2$ for lithium-ion secondary batteries", *J. Appl. Electrochem.*, **38** (2008) 1477–1481.
18. T.D. Ge, C.J. Long, L.Q. Yu, T.A. Dong, H.K. Long,

H. Yi, J.X. Yang, "Synthesis and characterization of $LiCo_{0.3-x}Ga_xNi_{0.7}O_2$ (x = 0, 0.05) as a cathode material for lithium ion battery", *Mater. Chem. Phys.*, **100** (2006) 217–223.
19. P.Y. Liao, J.G. Duh, S.R. Sheen, "Microstructure and electrochemical performance of $LiNi_{0.6}Co_{0.4-x}Mn_xO_2$ cathode materials", *J. Power Sources*, **143** (2005) 212–218.
20. J.H. Kim, Y.K. Sun, "Electrochemical performance of $Li[Li_xNi_{(1-3x)/2}Mn_{(1+x)/2}]O_2$ cathode materials synthesized by a sol-gel method", *J. Power Sources*, **119** (2003) 166–170.
21. C.J. Jafta, K. Raju, M.K. Mathe, N. Manyala, K.I. Ozoemena, "Microwave irradiation controls the manganese oxidation states of nanostructured ($Li[Li_{0.2}Mn_{0.52}Ni_{0.13}Co_{0.13}Al_{0.02}]O_2$) layered cathode materials for high-performance lithium ion batteries", *J. Electrochem. Soc.*, **162** (2015) A768–A773.
22. D. Aurbach, O.S. Lavi, C. Ghanty, M. Dixit, O. Haik, M. Talianker, Y. Grinblat, N. Leifer, R. Lavi, D.T. Major, G. Goobes, E. Zinigrad, E.M. Erickson, M. Kosa, B. Markovsky, J. Lampert, A. Volkov, J.Y. Shin, A. Garsuch, "Studies of aluminum-doped $LiNi_{0.5}Co_{0.2}Mn_{0.3}O_2$: Electrochemical behavior, aging, structural transformations, and thermal characteristics", *J. Electrochem. Soc.*, **162** (2015) A1014–A1017.
23. C. Pouillerie, L. Croguennec, C. Delmas, "The $Li_xNi_{1-y}Mg_yO_2$ (y = 0.05, 0.10) system: Structural modifications observed upon cycling", *Solid State Ionics*, **132** (2000) 15–29.
24. C.H. Chen, J. Liu, M.E. Stoll, G. Henriksen, D.R. Vissers, K. Amine, "Aluminum-doped lithium nickel cobalt oxide electrodes for high-power lithium-ion batteries", *J. Power Sources*, **218** (2004) 278–285.
25. Unit-Cell Software for Cell Refinement Method of TJB Holland & SAT Redfern, 1995.
26. J.K. Ngala, A.N. Chernova, M. Ma, M. Mamak, P.Y. Zavalij, M.S. Whittingham, "The synthesis, characterization and electrochemical behavior of the layered $LiNi_{0.4}Mn_{0.4}Co_{0.2}O_2$ compound", *J. Mater. Chem.*, **14** (2004) 214–220.
27. H. Kitaura, A. Hayashi, K. Tadanaga, M. Tatsumisago, "Electrochemical performance of all-solid-state lithium secondary batteries with Li-Ni-Co-Mn oxide positive electrodes", *Electrochim. Acta*, **55** (2010) 8821–8828.
28. W. Cho, S.M. Kim, K.W. Lee, J.H. Song, Y.N. Jo, T. Yim, H. Kim, J.S. Kim, Y.J. Kim, "Investigation of new manganese orthophosphate $Mn_3(PO_4)_2$ coating for nickel-rich $LiNi_{0.6}Co_{0.2}Mn_{0.2}O_2$ cathode and improvement of its thermal properties", *Electrochim. Acta*, **198** (2016) 77–83.
29. Y.K. Sun, I.H. Oh, "Synthesis of $LiNiO_2$ powders by a sol-gel method", *J. Mater. Sci. Lett.*, **16** (1997) 30–32.
30. H.U. Kim, J. Song, D.R. Mumm, M.Y. Song, "Effects of Zn or Ti substitution for Ni on the electrochemical properties of $LiNiO_2$", *Ceram. Int.*, **37** (2011) 779–782.
31. S.S. Julien, S. Michael, S. Ziolkiewicz, "Structural and electrochemical properties of $LiNi_{0.3}Co_{0.7}O_2$ synthesized by different low-temperature techniques", *Int. J. Inorg. Mater.*, **1** (1999) 29–37.
32. A. Rougier, G.A. Nazri, C. Julien, "Vibrational spectroscopy and electrochemical properties of $LiNi_{0.7}Co_{0.3}O_2$ cathode material for rechargeable lithium batteries", *Ionics*, **3** (1997) 170–176.
33. K. Ding, Y. Zhao, L. Liu, Y. Li, L. Liu, L. Wang, X. He, Z. Guo, "Significant role of "burned" graphene in determining the morphology of $LiNiO_2$ prepared under the air conditions", *Electrochim. Acta*, **176** (2015) 240–248.
34. J.G. Thevenin, R.H. Muller, "Impedance of lithium electrodes in a propylene carbonate electrolyte", *J. Electrochem. Soc.*, **134** (1987) 273–280.
35. N. Takami, T. Ohsaki, K. Inada, "The impedance of lithium electrodes in $LiPF_6$-based electrolytes", *J. Electrochem. Soc.*, **139** (1992) 1849–1854.
36. G.T.K. Fey, Z.X. Weng, J.G. Chen, T.P. Kumar, "Electroanalytical studies on sol-gel derived $LiNi_{0.8}Co_{0.2}O_2$", *Mater. Chem. Phys.*, **82** (2003) 5–15.
37. F. Croce, F. Nobili, A. Deptula, W. Lada, R. Tossici, A. Depifanio, B. Scrosati, R. Marassi, "An electrochemical impedance spectroscopic study of the transport properties of $LiNi_{0.75}Co_{0.25}O_2$", *Electrochem. Commun.*, **1** (1999) 605–608.
38. M.D. Levi, K. Gamolsky, D. Aurbach, U. Heider, R. Oesten, "On electrochemical impedance measurements of $Li_xCo_{0.2}Ni_{0.8}O_2$ and Li_xNiO_2 intercalation electrodes", *Electrochim. Acta*, **45** (2000) 1781–1789.
39. F. Nobili, R. Tossici, F. Croce, B. Scrosati, R. Marassi, "An electrochemical ac impedance study of $Li_xNi_{0.75}Co_{0.25}O_2$ intercalation electrode", *J. Power Sources*, **94** (2001) 238–241.
40. C. Nithya, V.S.S. Kumari, S. Gopukumar, "Synthesis of high voltage (4.9 V) cycling $LiNi_xCo_yMn_{1-x-y}O_2$ cathode materials for lithium rechargeable batteries", *Phys. Chem. Chem. Phys.*, **13** (2011) 6125–6132.